Prediction of Global Ionosphere TEC base on Deep Learning

Zhou Chen[1,2], Wenti Liao [1,2], Haimeng Li [1,2], Jinsong Wang[3], Xiaohua Deng[1,2], Sheng Hong[2]

[1]Institute of Space Science and Technology, Nanchang University, Nanchang, China

[2]Information Engineering School, Nanchang University, Nanchang, China

[3]Key Laboratory of Space Weather, National Center for Space Weather, Meteorological Administration, Beijing, China

Correspondence to: Haimeng Li, lihaimeng@ncu.edu.cn

Abstract

Ionospheric Total Electron Content (TEC) prediction has important reference significance for the accuracy of global navigation satellite systems (GNSS) based global positioning system, satellite communications and other space communications applications. In the study, an available prediction model of global IGS-TEC map is established based on testing several different LSTM-based algorithms. We find that Multi-step auxiliary algorithm based prediction model performs the best. It can precisely predict the global ionospheric IGS-TEC in the next 6 days (the MAD and RMSE are 2.485 and 3.511 TECU, respectively). Then, the autoencoder network algorithm is adopted to construct an assimilation model that transforming IGS-TEC map to MIT-TEC map. In order to judge the validity of the assimilation model, the outputs of the assimilation model are evaluated and compared with the IRI2016 model in four different geomagnetic storm events. It seems that the assimilation model can accurately forecast MIT-TEC by inputting the predicted IGS-TEC value. The performance of assimilation model for the predicting MIT-TEC is better than that of IRI2016.

Introduction

As the total electron content (TEC) is an important ionospheric parameter used for characterizing the dynamic process in ionosphere [Liu et al., 2020], the global TEC map is a very effective tool to monitor the ionospheric behavior. It is very helpful to study the global ionospheric response to extreme space weather (e.g. geomagnetic storm [Taylor and Earnshaw, 1969; Essex et al., 1981]). Thus, plenty of researchers try to construct effective methods to predict ionospheric TEC map in previous studies. Basing on the least squares collocation method, Schaer (1999) extrapolate the spherical harmonics coefficients to fit the TEC map in the previous 30 days to predict the overall TEC parameters for the next 2 days. Liu and Gao (2004) explore a multiple-layer tomographic method for ionospheric modeling over a local area GPS reference network to predict TEC.

However, the variation of ionosphere is mainly contributed to the solar wind intensity and geomagnetic activity, only using historical ionospheric TEC to predict future TEC (as presented in above studies) may have great limitations. By considering the values of Kp, Dst, and Ap indices, some research apply several Autoregressive orders and the Discrete Cosinus Transform (DCT) to obtain a better correlation between past and future TEC values [García-Rigo et al., 2009, 2011]. Wang et al. (2018) develop an adaptive autoregressive model to predict the global TEC map, the result shows that the difference between local TEC data obtained from IGS GIMs and JASON is approximately 3 TECU in low solar activity, and it can be greater than 6 TECU in mid-to-high solar activity.

Different from above traditional methods, the neural networks (NN) is one kind of data-driven technology, it can effectively absorb the plenty of information from big data, so many important features of data can be well reproduced using NN. In previous studies, Tulunay et al. (2006) adopt the Middle East Technical University Neural Network (METU-NN) model to predict ionospheric TEC. Habarulema et al. (2011) take advantage of the potential extrapolation capabilities and limitations of Artificial Neural Networks (ANN) to construct a South African regional TEC prediction model through determining the relationship between multiple inputs (sunspot number, averaged magnetic A index values and so on) and TEC. The results show that ANN extrapolates relatively well during quiet periods, but the accuracy of prediction is lower during geomagnetic disturbance period. Deep learning is a technology originated from NN, owning to the big data era, it has the chance to show its powerful data-learning ability. It has been widely used in the prediction of ionospheric TEC. Taking into account two closely related parameters: F10.7 and AP, Sun et al. (2017) propose a model based on long short-term memory (LSTM) to predict ionospheric vertical TEC of Beijing. Boulch et al. (2018) propose a Deep Neural Networks (DNNS) based method to forecast a sequence of global TEC maps through inputting consecutive sequence of TEC maps without introducing any prior knowledge other than rotation periodicity of Earth. Using six input parameters (including Kp index, solar flux, longitude and latitude, day of year, and time of day), Pérez et al. (2019) construct a global TEC prediction model on account of multi-layer perceptron (MLP) to forecast the global TEC in the next one day or several days. Chen et al. (2019) build a novel regularized DCGAN (R-DCGAN) algorithm to fill the missing data in MIT-TEC maps.

Actually the researches concerning the ionospheric TEC map prediction are far more than listed above, these studies prove that deep learning algorithms are a promising way to achieve high-precise ionospheric prediction. As is well known to all, data is the foundation of deep learning, its performance is highly dependent on training data, thus global TEC map prediction need high-quality global TEC data. However, it is a challenge to obtain global TEC map from entirely real observation, as the distribution of GPS stations are not uniform on the earth, and the observation of TEC is always missing on the ocean. As a result, the MIT-TEC map, which is obtained from realistic observation, is missing in

many places. In order to solve this problem, the IGS-TEC try to produces whole global TEC map by applying many technologies [Hernández-Pajares et al., 2008]. Although both of them are widely used for various ionospheric research, comparing IGS-TEC map with MIT-TEC map in some special region, a significantly bias can be found between them [Chen et al., 2019; Vierinen et al., 2015; Liu, 2011; Rideout and Coster, 2006; Chen et al., 2015; Chen et al., 2017]. On one hand, the IGS-TEC map supplies global coverage data, so it provides a good opportunity to predict the spatial and temporal feature of global ionospheric TEC for utilizing the IGS-TEC maps as training data in some deep learning algorithms. On the other hand, there are some missing observation regions in MIT-TEC map, but its observation is closer to real TEC value than that obtained from IGS-TEC map [Aa, et al., 2015; Chen et al., 2019]. Therefore, the MIT-TEC value is generally considered as ground truth. The goal of this paper is to build a conversion relationship from IGS-TEC to MIT-TEC by deep learning algorithms, and construct a method (applying multiple deep learning algorithms) to produce the predicted TEC map with global coverage. The predicted value is as close as possible to MIT-TEC value.

The paper is structured as follows: The section 2 introduces the data set, its processing and technology guideline. The study of global IGS-TEC map predictions due to four different LSTM-based algorithms are presented in Section 3. The assimilation model based on Autoencoder is proposed in section 4, and the assimilation model will be further tested the validity during both geomagnetic quiet and storm periods. The summary and discussion are given in section 5. Finally, the detail of above algorithms can be referred in the Appendix A of this paper.

Data and Methods

In this work, the TEC data is obtained from two institutions. One is TEC grid data from International GNSS service (IGS) center with 1-hour time resolution. The other one is the vertical TEC data from the MIT Haystack Madrigal dataset (http://madrigal.haystack.mit.edu/). The grid size of both TEC map is processed to 64×64. The MIT-TEC cannot cover the global, the missing data in these TEC images accounted for one third of the total. Furthermore, the missing observation locations aren't exactly the same at different times. In order to improve the accuracy of prediction, four parameters obtained from OMNI dataset with 1 hour time resolution, including the sunspot number R, the solar radio flux F10.7, the geomagnetic activity index Ap, and the geomagnetic storm index Dst, are used as external geophysical driving source and are input into the auxiliary algorithm to improve the predicting performance.

In the study, the TEC data and OMNI data covers from January 2011 to December 2019. During such a long period, ionospheric periodic variations are very abundant. Figure 1 shows the daily and annual average variation of global overall ionospheric TEC from 2011 to 2019, which is obtained from IGS-TEC. Apparently, the TEC value obviously varied as a function of time. As a result,

dividing the total data into the training set, validation set, and test set should be different from traditional data processing method. Actually, in order to make them with the same distribution as possible, a cycle of 90-day is employed in the study, where the first 30 days are considered as the training set, the middle 30 days are considered as the validation set, and the last 30 days are considered as the test set.

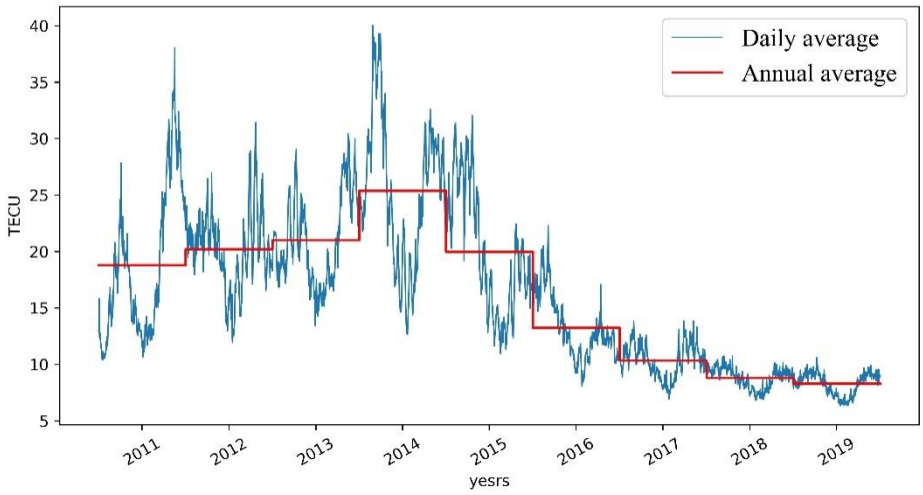

Figure 1. Daily and annual averages of all global IGS-TEC value in the dataset during the period from January 2011 to December 2019.

In this way, over 73000 sequences of TEC map for training, validation and testing are built. For TEC data, the time span of each sequence is 96 hours. The first 48 hours are used as the history data and input into the network. The future 1 hour or 48 hours TEC value will be predicted by multiple models. Each sequence of corresponding parameters includes 3 consecutive days of history OMNI data. Since the original time resolution (and range) of different OMNI data are divergent, in order to make influence of the four OMNI parameters consistent, the standardization processing to make different feature variables have the same scale and eliminate the differences of dimension between features which can speed up the convergence of weight parameters.

The goal of the constructed model is to predict the TEC for a period of time in the future interval through the history global ionospheric TEC sequence. Since ionosphere is an open system, its future behavior is not only inferred from its previous state, but also decided by the other driving source (e.g. solar and geomagnetic activities), in the study, the geophysical parameters obtained from OMNI are further input into the model to correct the error stacking caused by long-term prediction. In this paper, the final fusion model is established by two steps as follow. As shown in Figure 2, the first step is to construct the

prediction models of global ionospheric IGS-TEC map through four different LSTM-based algorithms, which are single-step self-prediction model, single-step auxiliary prediction model, multi-step self-prediction model and multi-step auxiliary prediction model (their detail algorithm can be referred to Appendix A). The self-prediction model only take advantage of corresponding historical TEC data to predict the future TEC map. And the auxiliary prediction model further considers above mentioned geophysical parameters (solar and geomagnetic activity index) as additional input data, including F10.7, R, Dst, and Ap indices values. In the study, the impact of the prediction times size on performance is also considered. The single-step prediction model only predicts the TEC data for one hour in the future each time, while the multi-step prediction model can predicts the TEC data for 48 hours in the future. Then each prediction model will be evaluated based on on the test set. The mean absolute deviation (MAD), root mean square error (RMSE) and coefficient of determination (R^2) are used as evaluation indicators. And the performance of those prediction models are compared in different seasons and years. As there is a systematic bias between the TEC provided by IGS and that provided by MIT, in order to render the deep learning model have the ability to predict MIT-TEC (in Figure A6 of Appendix A), in the second step, the autoencoder network is applied to construct an assimilation model that transform IGS-TEC to MIT-TEC, which finally realize the prediction of MIT-TEC. The performance of the MIT-TEC prediction model is evaluated in four geomagnetic storm events in 2020 by comparing with the International Reference Ionosphere (IRI2016 model.

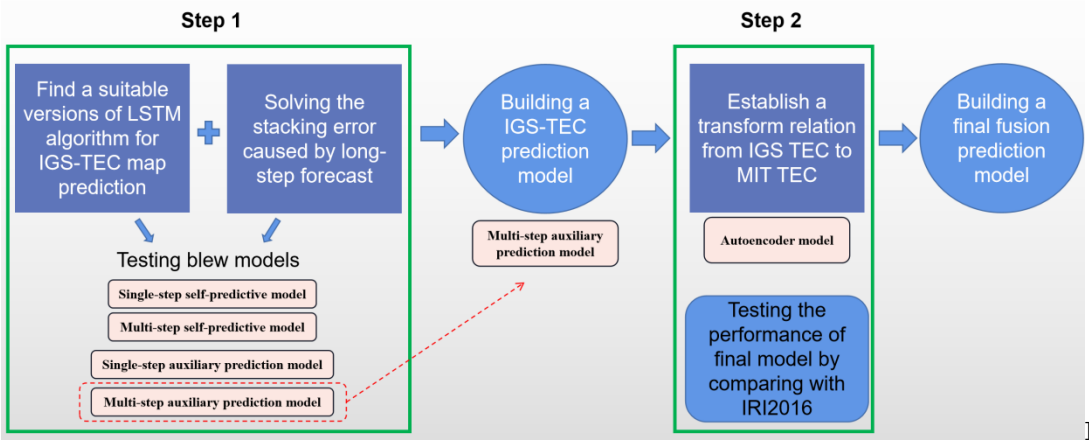

Figure 2. The technology guideline of this research.

Prediction for IGS map (Step 1)

3.1 Model Performance in Space

As the procedure of method presented in section 2, an example of global ionospheric TEC prediction models based on four different LSTM algorithms are shown in Figure 3. The start time of predicted global TEC map is at 15:00

UT on December 5, 2017. The length of predicted interval of TEC map is 144 hours. Comparing with two other models, the predicted TEC map obtained from multi-step and auxiliary prediction models are much closer to original realistic IGS-TEC map.

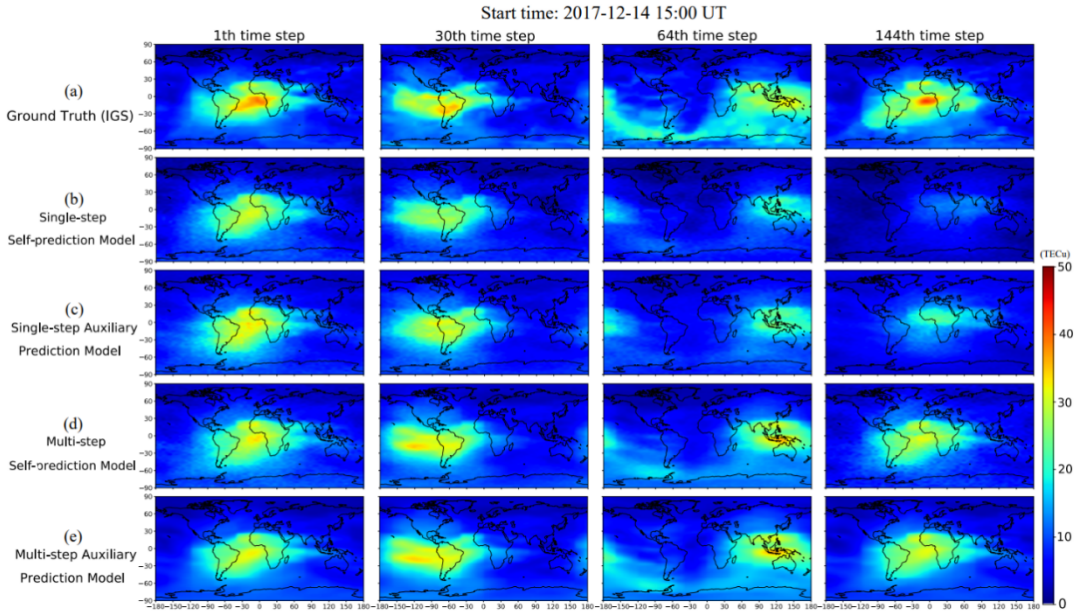

Figure 3. Row (a): the real obtained IGS-TEC map from 2017-12-14 15:00 UT on December 14, 2017 to next 144 hours. Row (b), (c), (d) and (e): the corresponding prediction of IGS-TEC map during the time interval through four different prediction models. (The details of the Single-step Self-prediction Model can be referred to the Section 1.1 of the Appendix A; The details of the Single-step Auxiliary Prediction Model can be referred to the Section 1.2 of the Appendix A; The details of the Multi-step Self-prediction Model can be referred to the Section 1.3 of the Appendix A; The details of the Multi-step Auxiliary Prediction Model can be referred to the Section 1.4 of the Appendix A.).

Since validations of the prediction models need more scientific evaluation indicators, in order to accurately evaluate the reliabilities and effectivenesses of models, several important evaluation indicators, including MAD, RMSE, and R^2 are used to evaluate the bias between the predicted value of four models and the IGS-TEC. Their mathematical expressions can be referred as follows:

where F_i represents the forecasted value, O_i represents the observed value, $\overline{F}$ and $\overline{O}$ are the mean values of F_i and O_i, respectively, n is equal to the number of grids in each TEC map.

The performance evaluation of four models on MAD, RMSE and R^2 are shown in Figure 4. Obviously, for all models, MAD and RMSE increase with the

enhancement of the prediction time, on the other hand, R^2 decreases with the enhancement of the prediction time. Most notably, the lower MAD and RMSE (or higher R^2) indicate that the model perform better. It suggests that the longer interval after the start time of prediction, the accuracy is lower. This is the limitation of LSTM-based prediction model, the errors in the rolling prediction gradually stack. However, the performance of the four models are different under the same testing condition. Apparently, the multi-step auxiliary model show the best performance under the three evaluation indicators, and the single-step self-prediction model is the worst.

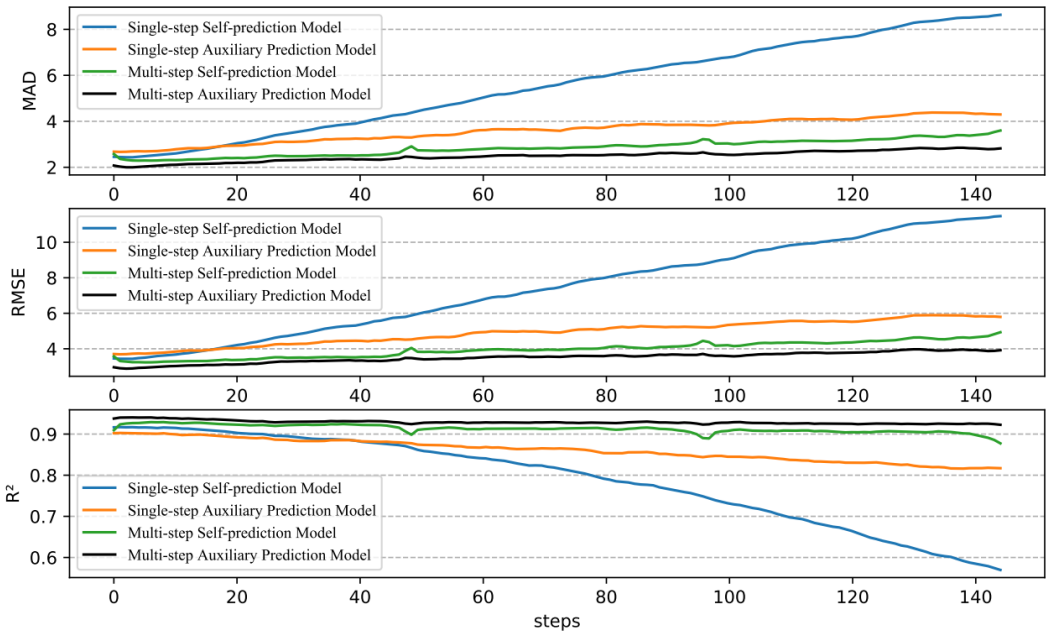

Figure 4. Three evaluation indicators (MAD, RMSE and R^2) are used to test the performance of prediction models.

In order to quantitatively prove the performances of the models, as exhibited in Table 1, the averaged estimation indicators of the global ionospheric TEC are calculated due to different models for the next 24 hours, 48 hours, and 144 hours, respectively. In the predicted interval within 24 hours, the single-step auxiliary (multi-step auxiliary) model performs the worst (best) among the four models, but overall, the differences are subtle. However, with the prediction interval increases, the differences among the models gradually gain. Comparing with the interval within 24 hours, the averaged MAD (RMSE) values calculated from the single-step self-prediction model within 48 hours increased from 2.721 (3.806) TECu to 3.259 (4.483) TECu. The averaged R^2 value dropped from 0.911 to 0.899. For the multi-step auxiliary prediction model, this change over interval of prediction is much smaller. The averaged MAD (RMSE) values only increased

by 0.109 (0.142) TECu, the averaged R^2 value only dropped by 0.008. After increasing the prediction time to 144 hours, the performed difference of the four models are further enlarged. Comparing with other models, the performance degradation of the multi-step self-prediction model is much smaller than others. On the whole, in terms of reducing the deviation caused by the error stacking with predicted time increasing, the performance of multi-step prediction model is better than that of single-step prediction model, and the auxiliary prediction model is better than the self-prediction model.

Table 1. The performance of models on the test set

Models	24h (average)			48h (average)			144h (average)		
	MAD (TECu)	RMSE (TECu)	R^2	MAD (TECu)	RMSE (TECu)	R^2	MAD (TECu)	RMSE (TECu)	R^2
single-step self-prediction model									
single-step auxiliary prediction model									
multi-step self-prediction model									
multi-step auxiliary prediction model									

Figure 5 shows the global distribution of MAD and RMSE when the four models predict the global ionospheric TEC in the time interval of next 1 hour, 24 hours, 64 hours and 144 hours. It reflects that the abilities of above models to reduce error stacking with prediction time increasing are significantly different. In the predicted time interval from the 1th to 24th hour, the largest value of MAD and RMSE can be clearly found in the geomagnetic latitude 15°N 25°N and 15°S 25°S, which is belong to the area of equatorial ionospheric anomaly. This result may be caused by the complicated physical mechanism in ionospheric equator anomaly region. However, the increase of predicted time enlarges the region with high MAD and RMSE for most models.. It is most obvious for the single-step self-prediction model while the predicted time is beyond 144th hour, the geophysical structure is completely lost in the condition. Luckily, as shown in the 4th and 8th rows of Figure 5, the Multi-step Auxiliary prediction model can effectively hinder this error stacking problem while the predicted time is less than 144 hours.

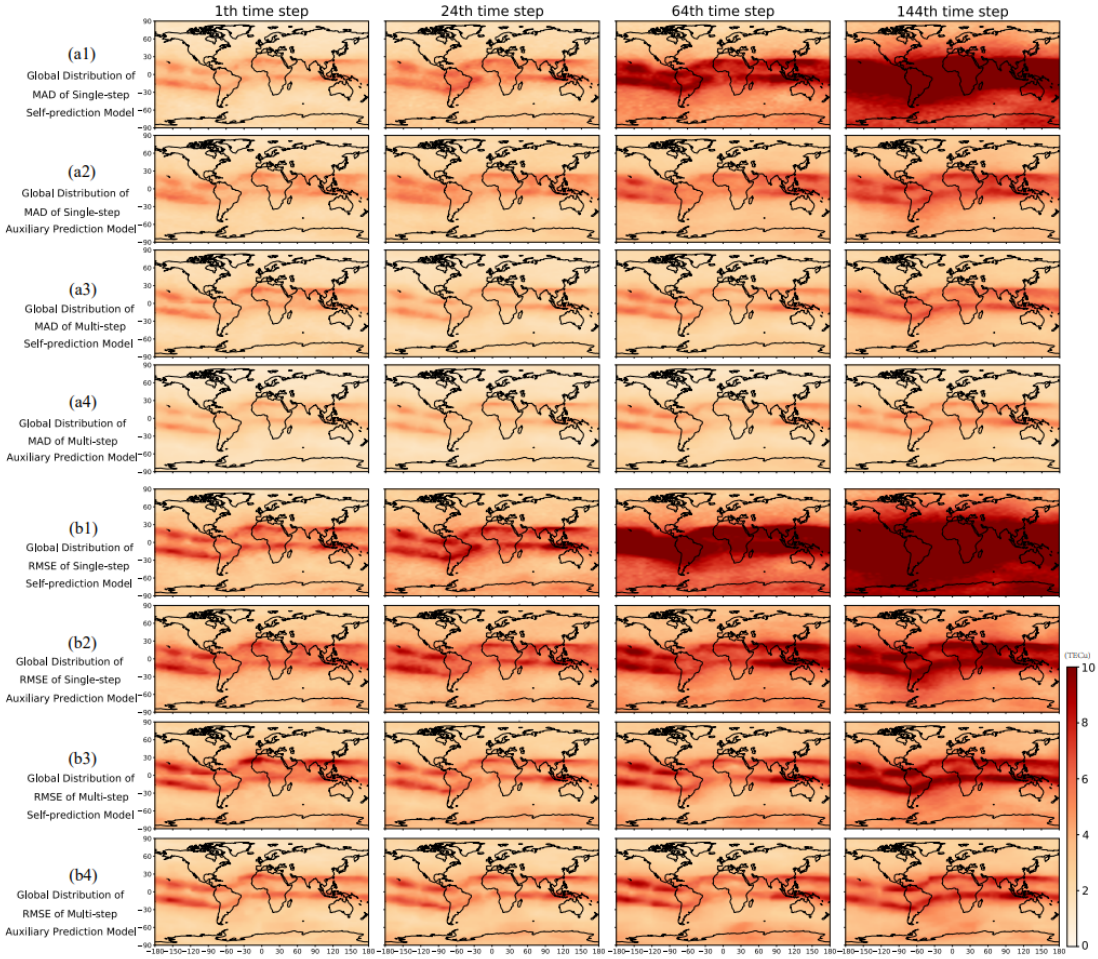

Figure 5. The global distribution of the MAD [(a1) to (a4)] and RMSE [(b1) to (b4)]

3.2 Model Performance in time

3.2.1 the performance in different Seasons

Many studies have shown that the performance of ionospheric TEC prediction models varies with the seasons [Mukesh et al., 2020; Tebabal et al., 2019]. Next, the performances of all proposed models above in different season and year are evaluated. The test set is divided into four parts by month: March to May regarded as spring, June to August regarded as summer, September to November regarded as autumn, and December to February regarded as winter. Figure 6 shows the performances of the four models in four seasons as a function of the length of predicted time. There is no doubt that the accuracies of all models in

any season decrease as the predicted time increases. However, it is worth to notice that the performance of four model show hug difference in different seasons. For the Single-step Self-predictive Model and Single-step Auxiliary Prediction Model, the performance of MAD and RMSE is the best in summer, and performance of R^2 is the best in winter. For the multi-step self-prediction model and the multi-step auxiliary prediction model, the performance of the three indicators is the best in spring. MAD and RMSE performed the worst in winter, and R^2 performed the worst in autumn. However, even if the performance of multi-step auxiliary prediction model is poorer in autumn and winter than other two seasons, it still perform better than the other three models. This shows that either adding OMNI data as the input predictive factors or increasing the single prediction step size can improve the performance of the global ionospheric TEC prediction model based on LSTM related algorithm.

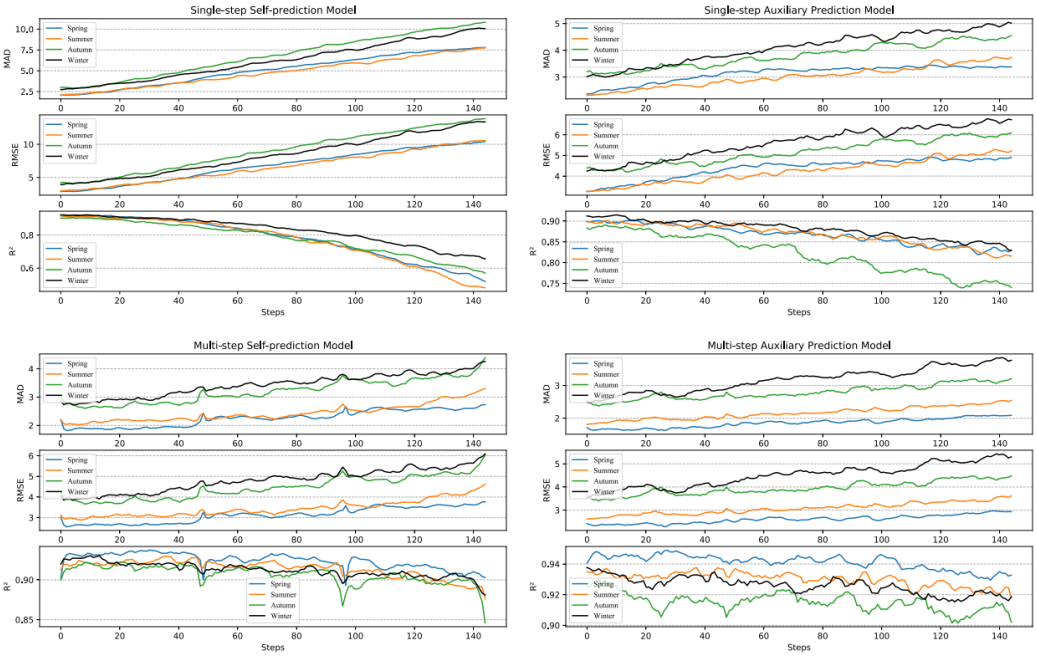

Figure 6. Models performance in different seasons

3.2.2 The performance in different years

As shown in Figure 1, the variation of ionospheric TEC is the most dramatic in 2014 and quietest in 2019, so in order to further study the prediction performance of four models under different years, all the four models are tested in 2014 and 2019, respectively. As shown in Figure 7, it implies that all models performed worse in 2014, this may be because that 2014 corresponds to high

year of solar activity, as more intense geomagnetic activity makes the variations of the ionosphere more complicated. But either in 2014 or 2019, Multi-step Auxiliary Prediction Model is the best performing model. Comparing with the result in 2019, the Multi-step Auxiliary Prediction Model in 2014 reduced about 2 TECUs in MAD, reduced less than 3 TECUs in RMSE, and almost keep stable in R^2 value.

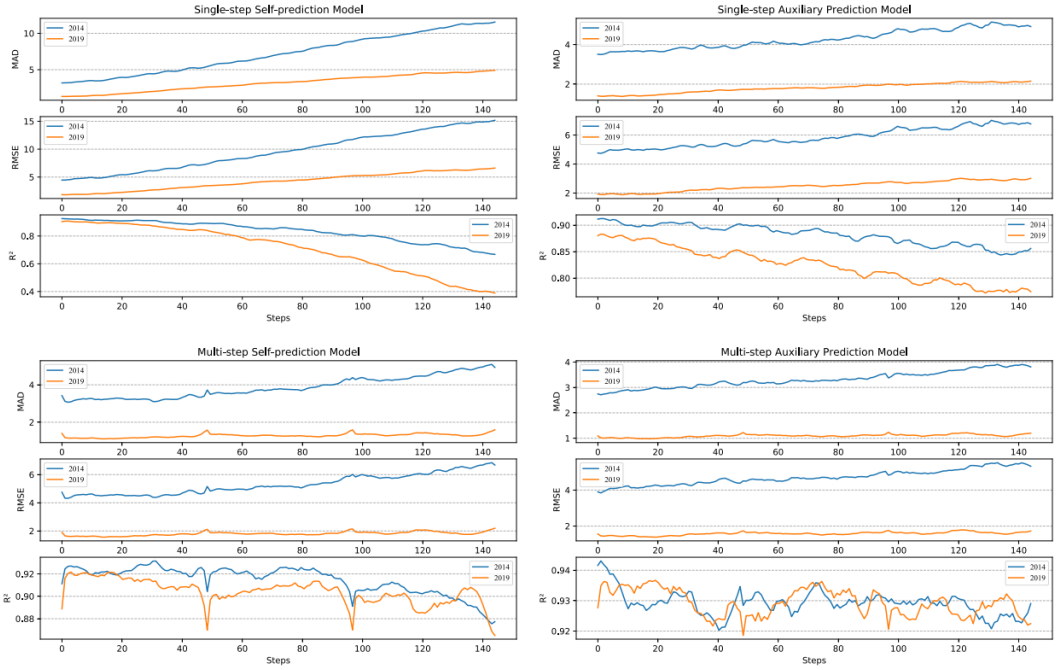

Figure 7. Models performance in different years

Assimilation model from IGS to MIT TEC (Step 2)

The results presented above can be concluded that the Multi-step Auxiliary Prediction Model performs the best in predicting global ionospheric TEC. Therefore, the Multi-step Auxiliary Prediction Model is chosen as the basic model to further build the assimilation one. The training data set covers from 2011 to 2019, only the data obtained in 2020 are considered as validation dataset, however, there is no strong geomagnetic storm occurred in this year, so four relatively medium (-100 nT Dst -50 nT) geomagnetic storm events are selected to evaluate the practicality of the models. Meanwhile, in order to make the evaluation results of the model comparable, the result calculated from International Reference Ionospheric model (IRI2016) is considered as a reference, and compare with the result from our model.

4.1 The Performance of Testing Model in quiet period

Actually, the goal of Assimilation model is to establish the transform relationship from IGS-TEC to MIT-TEC with global coverage by applying the Autoencoder algorithm (the detail algorithm structure can be referred to the Figure A6 in Appendix A), and the outputs of IGS-TEC prediction model are considered as the inputs of Assimilation model. In order to validate the preciseness of the assimilation model, another widely-used ionospheric prediction, IRI2016 model, is chosen as referenced model. In Figure 8a, the realistic MIT-TEC maps from 00:00 UT on May 25, 2020 to the next 144th hour are exhibited. It is worth noting that the missing observation regions are diverse in different time. Meanwhile, the predicted global TEC map with global coverage from 00:00 UT on May 25, 2020 to the next 144th hour are calculated by Multi-step Auxiliary Prediction Model (as exhibited in Section 3), assimilation model and IRI2016 model, respectively. In order to clearly compare the predicted maps calculated from the three models with the realistic MIT-TEC observation, the TECs are exhibited only in the region where there are realistic observations (as shown in Figure 8b-d). It seems that the result obtained from assimilation model is more closer to MIT-TEC map than that calculated from IRI2016 during this geomagnetic quiet period (Dst -30 nT).

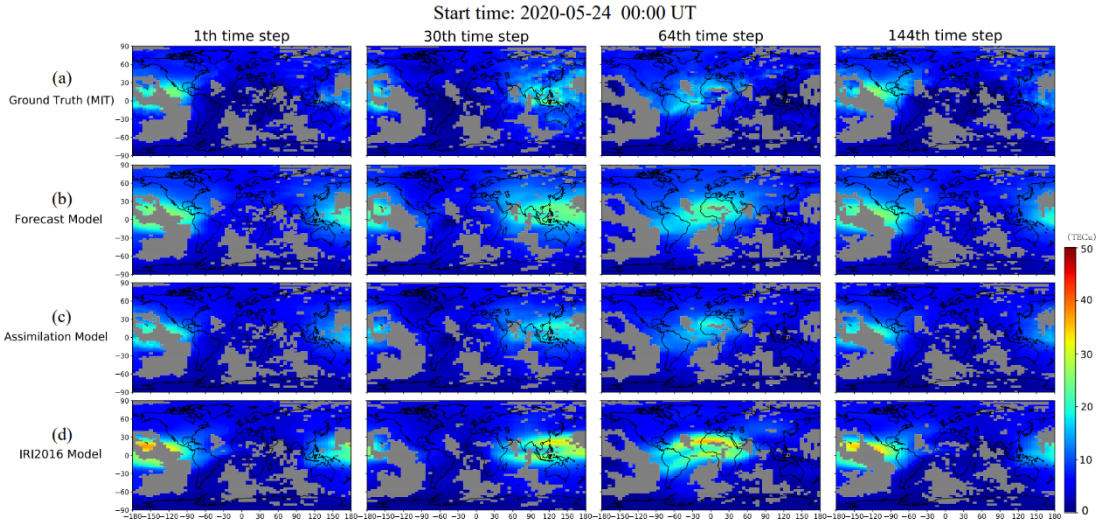

Figure 8. (a) The realistic MIT-TEC maps from 00:00 UT on May 25, 2020 to the next 144th hour. (b-d) The corresponding predicted global TEC map calculated from Multi-step Auxiliary Prediction Model, assimilation model and IRI2016 model, respectively. The details of the Assimilation Model can be referred to the Section 1.5 of the Appendix A.)

4.2 Performance of Testing Model in geomagnetic disturbance period

In order to reflect the generalization ability of the model, predicted TEC maps during four medium geomagnetic storm events in the year of 2020 are selected to evaluate the practicality of the models. While the MIT data are referred as the ground truth, the estimation indicators of the three models as a function of time during the four geomagnetic storms are calculated. As indicated in Figure 9, the black line denotes the variation of Dst value, the blue line represents the evaluation result calculated from the IRI2016 model, the orange line represents the evaluation result from the multi-step auxiliary prediction model, and the red line represents the evaluation result of assimilation model. It suggests that the performance of the forecast model is not as good as that of IRI2016 for most of the time before assimilation. One of the main reasons is that our forecast model is trained and tested with IGS-TEC. In other words, the forecast model just fits the data of IGS-TEC other than that of MIT-TEC. Furthermore, there is an obvious systematic error between IGS-TEC and MIT-TEC. So before the assimilation, in the condition while using MIT-TEC as realistic vertical TEC to measure the performance of the model, the performance of model is a bit worse than IRI2016. But in the condition while assimilating the prediction results by the Autoencoder algorithm, the performance can be significantly improved, and it is even better than IRI2016 for most of the time.

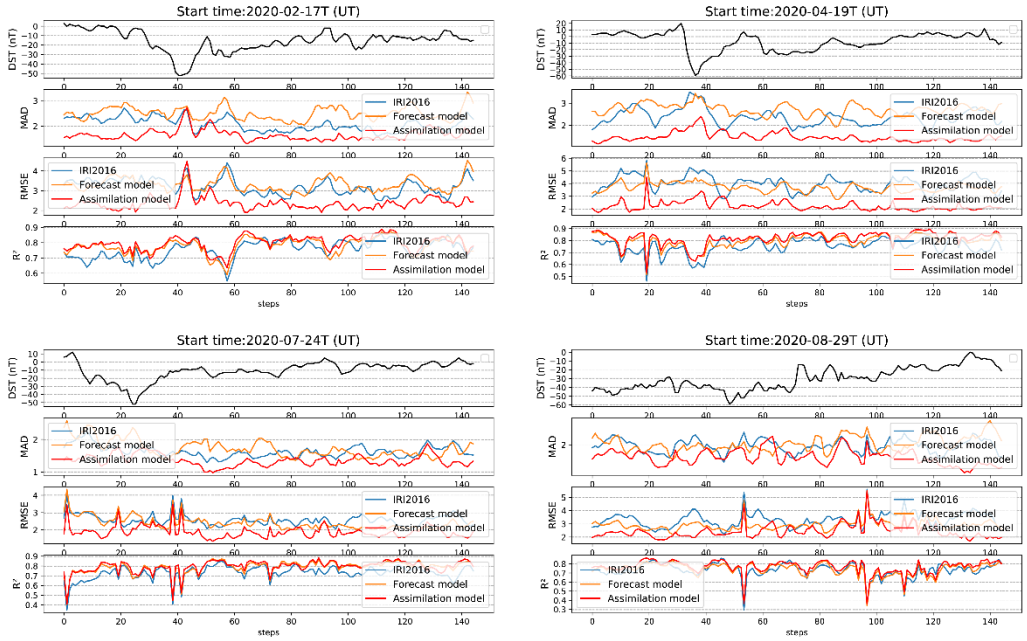

Figure 9. The performance of models in four geomagnetic storm events

Discussion and Summary

In this paper, there are two steps to construct a relatively precise prediction model of global TEC map that closes to MIT-TEC observation. Firstly, IGS-TEC map prediction models are constructed by four LSTM-based algorithms. Then the accuracies of the models are tested in different predicted time length. It suggests that the accuracy of auxiliary prediction model is much higher than the self-prediction model through importing extern geomagnetic and solar activity indexes (including F10.7, R, Dst, and Ap indices values). Furthermore, comparing with the single-step prediction model which only forecasts the global ionospheric TEC for one hour at a time, the multi-step prediction model can forecast the next 48 hours at a time. The multi-step prediction model significantly improves the accuracy of the forecast by reducing the error of rolling forecasts. It is obvious that the multi-step auxiliary prediction model can combine the both advantages of auxiliary algorithm and multi-step prediction model, and its accuracy of prediction has been further improved. As shown in Figure 4 and Table 1, the constructed multi-step auxiliary prediction model can accurately predict the global ionospheric TEC in the next 6 days, and the error rises very little.

Secondly, another kind of deep learning model: autoencoder network algorithm, is adopted to construct an assimilation model that transforms IGS-TEC map to MIT-TEC map. The performance of the model is evaluated in four different geomagnetic storm events in the year of 2020, and then the results is compared with the IRI2016 model. It seems that the assimilation model can better forecast MIT-TEC through importing the predicted IGS-TEC value from multi-step auxiliary prediction model (obtained from step 1). According to evaluating the performance of the model in four medium geomagnetic storm events, it suggests that the performance of constructed assimilation model in the study for the predicting MIT-TEC is better than that of IRI2016.

Based on above results, our conclusions are as follows:

1. The prediction error stacking with time increasing can be effectively weaken by adding multi-step prediction model and auxiliary algorithm. As is well known, ionosphere is an open system, its future behavior is not only inferred from its previous state, but also determined by the other extern driving sources (e.g. solar wind and geomagnetic activities). Thus the LSTM-based algorithm can reproduce ionospheric background variation, and auxiliary algorithm can effectively reflect ionospheric response to the effect of external driving resource.

2. Multi-step auxiliary prediction model can better predict the global ionospheric TEC in the next 6 days, and the error rises is very small (the MAD and RMSE are 2.485 and 3.511 TECU, respectively), when the training data is IGS-TEC.

3. When the testing data is completely separated from the training set, the

performance of assimilation model is proven to be better than IRI2016 under the condition that MIT-TEC is considered as ground truth. This advantage can be confirmed in both the geomagnetic quiet and storm period.

As a summary, either multi-step prediction model or auxiliary algorithm improve the prediction accuracy in time domain. Meanwhile, autoencoder network algorithm can enhance the prediction accuracy in space domain. Based on the above two technologies, we can obtain a better model of predicting MIT-TEC, which is obviously superior than that of IRI2016. However, our assimilation model is very preliminary. In future study, the improvement with parameters optimization or addition of other algorithms should be done. Furthermore, the dependence of the robustness of our model on different geomagnetic and solar conditions will be also studied.

Acknowledgments

The IGS TEC map data used in the present paper are from the Goddard Space Flight Center, space physics data facility, online at http://cdaweb.gsfc.nasa.gov/istp_public/. The MIT-TEC data are obtained from the MIT Haystack Madrigal data set (http://madrigal.haystack.mit.edu/). The Dst data used in present study are provided by World Data Center for Geomagnetism, Kyoto, online at http://wdc.kugi.kyoto-u.ac.jp/dstae/index.html, respectively. We thank these organizations for making their data public. The effort at the Nanchang University was supported by the National Natural Science Foundation of China (grants 41974183 and 41774195, 42064009).

Appendix A: The Architectures of four LSTM and Autoencoder algorithms

In the field of deep learning, Recurrent Neural Network (RNN) are widely used to process the data of time series. Because RNNs contain the procedure of loops, which can store information while processing new input. This kind of memory makes them very suitable for tasks that must be considered in advance. RNN can handle certain short-term dependencies, but cannot handle long-term dependencies, which will cause gradient disappearance and gradient explosion problems. LSTM is a variant of RNN network. Cell state is introduced on the basis of RNN. According to the cell state, it can decide which states should be kept and which states should be forgotten. It solves the long-term dependency problem of the general RNN network. LSTM uses forget gates, input gates, and output gates to maintain and control information from a microscopic point of view. The error function of selective memory feedback is corrected with the gradient drop to realize the memory function in time and prevent the gradient from disappearing. The calculation formula for a single time step of LSTM is as follows:

$$f_t = \sigma\left(W_f \bullet [h_{t-1}, x_t] + b_f\right) \#(A1)$$

$$i_t = \sigma\left(W_i \bullet [h_{t-1}, x_t] + b_i\right) \#(A2)$$

$$\widetilde{C_t} = tanh\left(W_C \bullet [h_{t-1}, x_t] + b_C\right) \#(A3)$$

$$C_t = f_t * C_{t-1} + i_t * \widetilde{C_t} \#(A4)$$

$$o_t = \sigma\left(W_o \bullet [h_{t-1}, x_t] + b_o\right) \#(A5)$$

$$h_t = o_t * \tanh\left(C_t\right) \#(A6)$$

Among them f_t is forget gate, i_t is the input gate, o_t is the output gate, $\widetilde{C_t}$ is the cell state candidate value, C_t is the cell state, h_{t-1} is the state value of the previous hidden layer, and x_t is the input at the current moment, W and b are weights and biases, and σ is the activation function.

In this work, we build four global Ionospheric TEC prediction models based on LSTM.

1.1 Single-step self-predictive model

The single-step self-prediction model only uses the TEC data of the past 48 hours, that is, the historical data does not contain other physical parameters (applies to section 2.3). In this model, we use four LSTM layers. The TEC map data is two-dimensional data. In order to match the input dimensions of the LSTM network, we need to flatten the TEC map. This model uses TEC data in the past 48 hours to predict the TEC in the next hour. The optimizer of the model is Root Mean Square prop (RMSProp) and the loss function is Mean Squared Error (MSE).

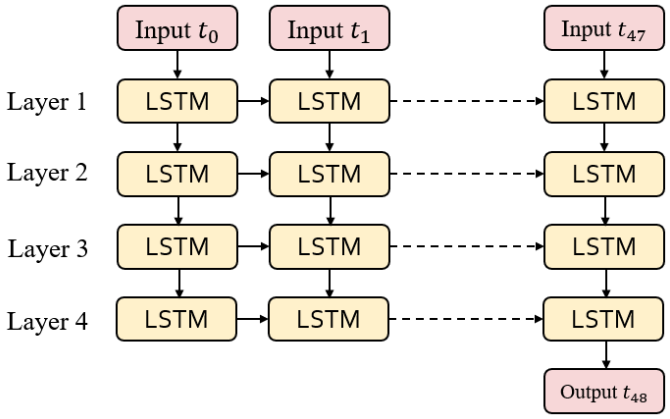

Figure A1. Single-step self-predictive model structure

1.2 Single-step auxiliary prediction model

The single-step auxiliary prediction model not only uses the past TEC data, but also uses three consecutive days of historical data of physical parameters as predictors. The input of this model is divided into main input and auxiliary input, namely continuous 48 hours of global ionospheric TEC historical observation data and three consecutive days of four physical parameters. The main input passes through four LSTM layers to get an auxiliary output. The auxiliary output is combined with the auxiliary input, and then the main output is obtained through two fully connected layers. Both outputs and observations can get their respective losses. The auxiliary loss function evaluation is only a prediction based on the ionospheric TEC data itself, and the main loss function evaluation is a prediction based on the TEC data and physical parameters. Here we give the auxiliary loss a weight of 0.2 and the main loss a weight of 1.0. In this way, even if the gradient from the main loss function is diffused, the information from the auxiliary loss function can train the LSTM layer. Here, we use RMSProp as the optimizer and MSE as the loss function.

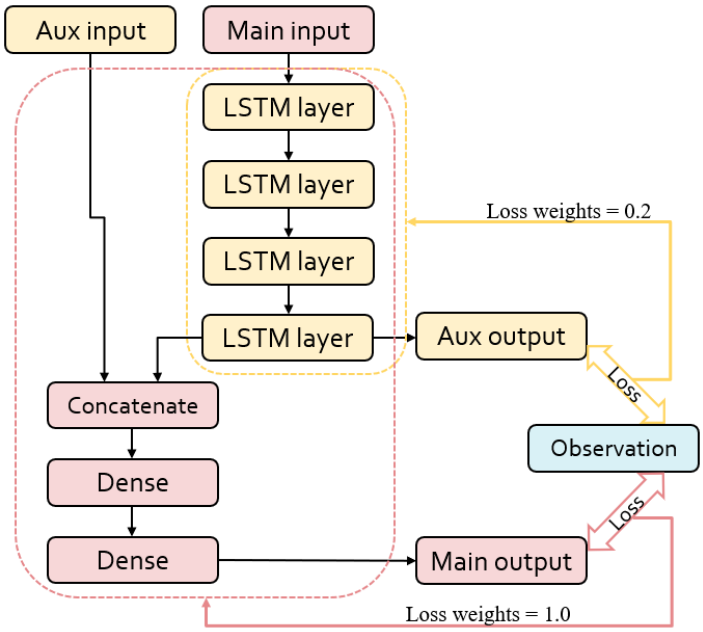

Figure A2. Single-step auxiliary predictive model structure

1.3 Multi-step self-predictive model

The models described in the two sections above are all single-step prediction models. The errors of long-term forecasts are mainly caused by the stacking of errors in rolling forecasts. Fixed prediction length, the longer the single-step prediction time, the fewer rolling predictions. For neural networks, adaptability is one of its advantages. For this model, we also only use the globe ionospheric TEC data in the previous 48 hours. The difference is that the output is no longer the TEC data of the next hour, but the next 48 hours. Here, we use RMSProp as the optimizer and MSE as the loss function.

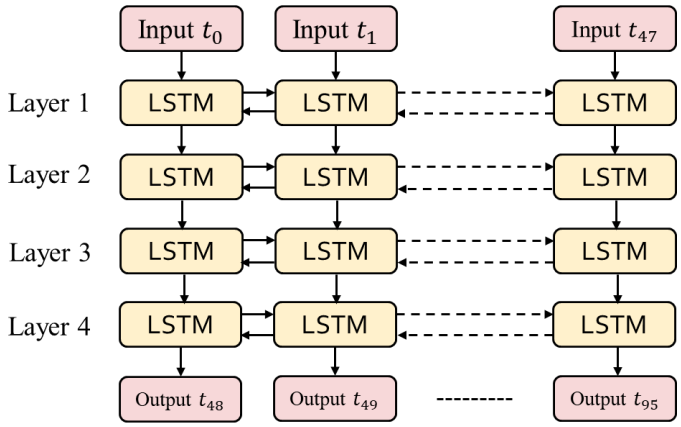

Figure A3. Multi-step self-predictive model structure It is worth noting that this model uses four Bidirectional LSTM (Bi-LSTM) layers. It can be seen from the macro structure diagram of the model that the *Output* t_{48} prediction information is actually passed and updated from the back end to the begin of the input sequence. If there is no reverse LSTM, the *Output* t_{48} will not be able to learn any evolution law of the TEC map time series. Similarly, *Output* t_{49} can only learn a very one-sided evolutionary law from the first two time steps of the input sequence. After adding reverse LSTM, these problems can be effectively solved.

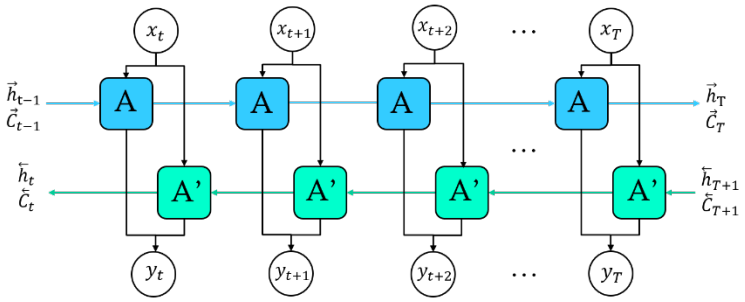

Figure A4. The structure diagram of Bi-LSTM layer. $\mathbf{x_i}$ represents the input at each time, $\mathbf{y_i}$ represents the output at each time and "A" represents the LSTM network unit. The calculation process of the Bi-LSTM network is as follows: (1) In the forward process, for the output at time t, the forward LSTM layer has the information of the input data x_i and the previous moment of the cell state $\overrightarrow{C}_{t-1}$ and the hidden layer output $\overrightarrow{h}_{t-1}$. (2) In the reverse process, for the output at time t, the reverse LSTM layer has the information of the input data x_i and the previous moment of the cell state $\overleftarrow{C}_{t+1}$ and the hidden layer output $\overleftarrow{h}_{t+1}$. (3) At time t, the output of the forward LSTM layer is denoted as $\overrightarrow{h}_t$, and the output of the reverse LSTM layer

is denoted as $\overleftarrow{h}_t$. The vector addition of the output of the two LSTM layers is the output of the hidden layer at time t, denoted as $\overrightarrow{h}_t + \overleftarrow{h}_t$. It is used as the input of the output layer, and the final output y_t is obtained through the softmax unit.

1.4 Multi-step auxiliary prediction model

The input of the multi-step auxiliary prediction model is the same as that of the single-step auxiliary prediction model. The difference is that the model can predict 48 hours of global TEC data at single time. This will help improve the accuracy of long-term prediction. In this model, the main input passes through four bidirectional LSTM layers then get the auxiliary output. The auxiliary output is combined with the auxiliary input, and the main output is obtained through a convolutional layer. Here, the reason why the fully connected layer is not used is that the output is 48 TEC map data instead of one. If a fully connected layer is used, the parameters of this layer will increase by 48 times, exceeding the maximum load of the hardware device. Like the single-step auxiliary prediction model, this model also has two loss functions. Here we give the auxiliary loss a weight of 0.2 and the main loss a weight of 1.0. And the Observations are no longer the global ionospheric TEC data for the next 1 hour, but 48 hours. Here, we use RMSProp as the optimizer and MSE as the loss function.

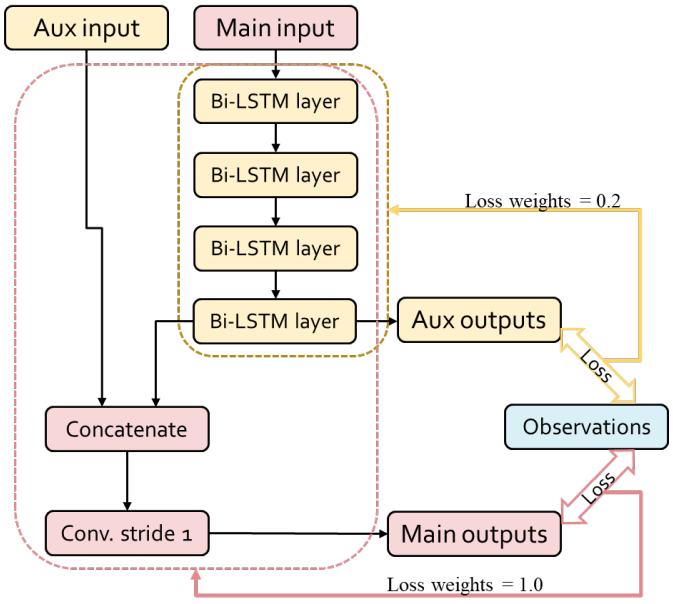

Figure A5. Multi-step auxiliary predictive model structure

1.5 Assimilation model

The ionospheric TEC provided by MIT does not cover the world, and the missing position is not constant. Therefore, the historical TEC cannot be used to predict the future TEC like the IGS-TEC forecast model.

The global ionospheric TEC prediction model based on LSTM can effectively predict the global ionospheric TEC, and the predicted TEC is close to the IGS standard instead of MIT. There is a systematic deviation between the ionospheric TEC data provided by IGS and MIT. In order to make the forecasted TEC is close to the MIT standard, we used an Autoencoder network to assimilate the TEC data provided by IGS and MIT. The structure of the Autoencoder model is shown in Figure 7. The Encode part of the model is composed of two Conv2D layers, and the Decode part is composed of two Conv2DTranspose layers. In the training phase, the inputs of the Autoencoder model is the global ionospheric TEC data provided by IGS, and the outputs is the global ionospheric TEC data with missing provided by MIT. It is worth noting that IGS data needs to be preprocessed before being input into the model: We assign '0' to partial positions of the TEC map provided by IGS, and these positions are the same as the missing positions of the MIT data at the same time. In the testing phase, the inputs of the model is the outputs of the global ionospheric TEC prediction model based on LSTM, and the outputs of the model is the assimilation result of the TEC data of IGS and MIT. In this model, the optimizer we use is Adam, and the loss function is MSE.

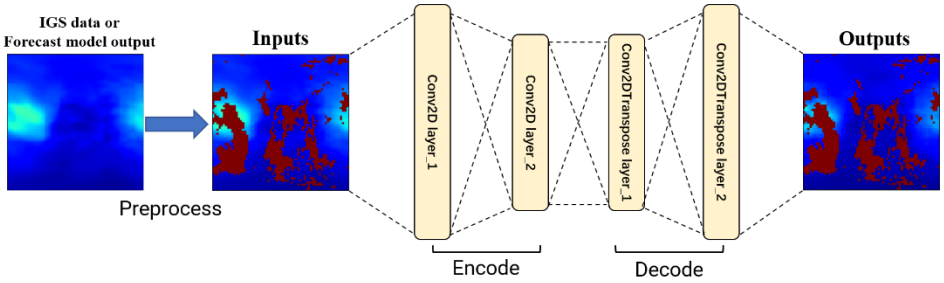

Figure A6. IGS-TEC and MIT-TEC assimilation model

References

Aa, E., W. Huang, S. Yu, S. Liu,L. Shi, J. Gong, Y. Chen, and H. Shen (2015), A regional ionospheric TEC mapping technique over China and adjacent areas on the basis of data assimilation, J. Geophys. Res. Space Physics, 120, 5049–5061, doi:10.1002/2015JA021140.

Boulch, A., Cherrier, N., & Castaings, T. (2018). Ionospheric activity prediction using convolutional recurrent neural networks. arXiv preprint arXiv:1810.13273.

Chen, Z., Zhang, S., Coster, A., and Fang, G. (2015). EOF analysis and modeling of GPS TEC climatology over North America. Journal of Geophysical Research, 120(4), 3118-3129, doi:10.1002/2014JA020837

Chen, Z., Wang, J., Deng, Y., and Huang, C. (2017). Extraction of the geomagnetic activity effect from TEC data: A comparison between the spectral whitening method and 28 day running median. Journal of Geophysical Research, 122, 3632-3639, doi:10.1002/2016JA023412

Chen, Z., Jin, M., Deng, Y., Wang, J. S., Huang, H., Deng, X., and Huang, C. M. (2019). Improvement of a deep learning algorithm for total electron content maps: Image completion. Journal of Geophysical Research: Space Physics, 124(1), 790-800, doi:10.1029/2018JA026167

Essex, E., Mendillo, M., Schödel, J.P., Klobuchar, J., Rosa, A., Yeh, K., Fritz, R., Hibberd, F., Kersley, L., Koster, J.R., Matsoukas, D., Nakata, Y., and Roelofs, T. (1981). A global response of the total electron content of the ionosphere to the magnetic storm of 17 and 18 June 1972. Journal of Atmospheric and Solar-Terrestrial Physics, 43, 293-306, doi:10.1016/0021-9169(81)90091-X

García-Rigo, A., Monte, E., Hernández-Pajares, M., Juan, J., Sanz, J., Krankowski, A., and Wielgosz, P. (2009). Prediction of Global Ionospheric TEC Maps: First results on a UPC forecast product. egu general assembly.

García-Rigo, A., Monte, E., Hernández-Pajares, M., Juan, J. M., Sanz, J., Aragón-Angel, A., and Salazar, D. (2011). Global prediction of the vertical total electron content of the ionosphere based on GPS data. Radio science, 46(06), 1-3, doi:10.1029/2010RS004643

Habarulema, J. B., McKinnell, L. A., and Opperman, B. D. (2011). Regional GPS TEC modeling; Attempted spatial and temporal extrapolation of TEC using neural networks. Journal of Geophysical Research: Space Physics, 116(A4), doi:10.1029/2010JA016269

Hernández-Pajares, M., Juan, J., Sanz, J., Orus, R., García-Rigo, A., Feltens, J., Komjathy, A., Schaer, S., and Krankowski, A. (2008). The IGS VTEC maps: a reliable source of ionospheric information since 1998. Journal of Geodesy, 83, 263-275, doi:10.1007/S00190-008-0266-1

Liu, L., Zou, S., Yao, Y., and Aa, E. (2020). Multi-scale ionosphere responses to the May 2017 magnetic storm over the Asian sector. GPS Solut 24(1), 26, doi:10.1007/s10291-019-0940-1

Liu, Z.. (2011). A new automated cycle slip detection and repair method for a single dual-frequency gps receiver. Journal of Geodesy, 85(3), 171-183, doi:10.1007/S00190-010-0426-Y

Liu, Z., and Gao, Y. (2004). Ionospheric tec predictions over a local area GPS reference network. GPS Solutions, 8(1), 23-29, doi:10.1007/s10291-004-0082-x

Mukesh, R., Karthikeyan, V., Soma, P., and Sindhu, P. (2020). Forecasting of

ionospheric tec for different latitudes, seasons and solar activity conditions based on oksm. Astrophysics and Space Science, 365(1), 1-23, doi:10.1007/s10509-020-3730-x

Pérez, R. O. (2019). Using TensorFlow-based Neural Network to estimate GNSS single frequency ionospheric delay (IONONet). Advances in Space Research, 63(5), 1607-1618, doi:10.1016/J.ASR.2018.11.011

Rideout, W., and Coster, A. (2006). Automated GPS processing for global total electron content data. GPS Solutions, 10(3), 219-228, doi:10.1007/S10291-006-0029-5

Schaer, S.. (1999). Mapping and predicting the earth's ionosphere using the global positioning system. Geod Geophys.arb.schweiz.

Sun, W., Xu, L., Huang, X., Zhang, W., Yuan, T., Chen, Z., & Yan, Y. (2017). Forecasting of ionospheric vertical total electron content (TEC) using LSTM networks. 2017 International Conference on Machine Learning and Cybernetics (ICMLC), 2, 340-344, doi:10.1109/ICMLC.2017.8108945

Taylor, G. N., and Earnshaw, R. D. S.. (1969). Changes in the total electron content and slab thickness of the ionosphere during a magnetic storm in june 1965. Journal of Atmospheric & Terrestrial Physics, 31(1), 211-216, doi:10.1016/0021-916

Tebabal, A., Radicella, S. M., Damtie, B., Migoya-Orue', Y., and Nava, B. (2019). Feed forward neural network based ionospheric model for the east african region. Journal of Atmospheric and Solar-Terrestrial Physics, 191, 105052, doi:10.1016/J.JASTP.2019.05.016

Tulunay, E., Senalp, E. T., Radicella, S. M., and Tulunay, Y. (2006). Forecasting total electron content maps by neural network technique. Radio science, 41(04), 1-12, doi:10.1029/2005RS003285

Vierinen, J., Coster, A., Rideout, W., Erickson, P., and Norberg, J. (2015). Statistical framework for estimating GNSS bias. Atmospheric Measurement Techniques, 9, 1303-1312, doi:10.5194/AMT-9-1303-2016

Wang, C., Xin, S., Liu, X., Shi, C., and Fan, L. (2018). Prediction of global ionospheric VTEC maps using an adaptive autoregressive model. Earth, Planets and Space, 70(1), 1-14, doi:10.1186/s40623-017-0762-8